Influence of select discharge parameters on electric field transients triggered in collisionless very high frequency capacitive discharges

Sarveshwar Sharma,[1] Nishant Sirse,[2, a)] Abhijit Sen,[3] Miles M. Turner,[2] and Albert R. Ellingboe[2]

[1)] *Institute for Plasma Research and HBNI, Bhat, Gandhinagar 382 428, India*

[2)] *School of Physical Sciences and NCPST, Dublin City University, Dublin 9, Republic of Ireland*

[3)] *Institute for Plasma Researchand HBNI, Bhat, Gandhinagar 382 428, India*

(Dated: 26 September 2019)

Self-consistent particle-in-cell simulations are carried out to investigate the effect of discharge voltage, driving frequency and extent of electrode gap on the formation of electric field transients. The shape of the electron energy distribution function (EEDF) into the bulk plasma and the nature of the mode transition in plasma density is presented for driving frequency range from 27.12 MHz to 80 MHz. The present results, taken in conjunction with our previous study[1] [Physics of plasmas 23, 110701 (2016)] that only looked at the driving frequency dependence in collisionless capacitive Ar discharges, provide a comprehensive and detailed account of the dynamics of such discharges over a multi-parameter operational space.

Keywords: collisionless, capacitive discharges, very high frequency, electric field transients, particle-in-cell

[a)]e-mail: nishudita1628@gmail.com

I. INTRODUCTION

Radio-frequency (RF) voltage and current waveforms applied directly to an electrode in capacitive discharges can sustain a plasma at a low gas pressure. In the region of the high-voltage capacitive sheath that forms between the bulk plasma and the electrode stochastic heating is the principal source of power absorption for electrons through interactions with the oscillating sheath. Such stochastic or collisionless heating in capacitive discharges has been widely reported in the literature[2–24]. In material processing industry in order to have uniform deposition/etching throughout the substrate it is essential to have control over some of the critical sheath plasma parameters such as the ion flux and the ion energy. In a conventional CCP device, the discharge is usually driven by a single frequency (usually 13.56 MHz) RF source and the device characteristics are governed by a number of plasma parameters all of which are coupled to each other. Now-a-days, capacitive discharges excited by frequencies up to a few tens of MHz or even higher are receiving increased attention in the field of industrial applications. In addition to distinct plasma chemistry[25], such a higher frequency range is applied in reactors to attain improved plasma processing rates with lesser damage to the substrate over a large zone of the wafer[26–29]. Due to rise in the discharge current for a particular discharge power and lower DC self-bias, a higher plasma density can be produced in the very high frequency (VHF) band (*i.e.* 30-300 MHz) operated CCPs. This leads to a high etch rate low-damage processing compared to low frequency plasma excitations.

The creation of electron beam from the vicinity of sheath edge that penetrate through the bulk plasma without collisions and interact with the opposite sheath can produce ionization and sustain the discharge in VHF driven CCP discharges[1,30,31]. These electron beams are responsible for the production of strong electric fields in the bulk plasma which was previously observed not only in electropositive and electronegative but also in symmetric and asymmetric CCP discharges[1,32]. Formation of multiple electron beams are also observed which depend on the driving frequency and discharge voltage[33,34]. Presence of higher harmonics in voltage and current are also reported in the literature of VHF CCP discharges[35,36]. Recently, Wilczek *et al.*[37] compared the results of current and voltage driven asymmetric capacitive discharges using particle in cell simulations in the regime of low pressure. Their simulation outcomes demonstrate that a voltage driven CCP generates higher frequency components in

the rf current, whereas, there are no higher harmonics in voltage for a current driven CCP. Most of these studies were performed in asymmetric CCP discharges.

Recently a very interesting phenomenon, namely, the formation of electric field transients associated with such higher frequency discharges at low pressures (collisionless regime) has been reported in numerical simulation studies[1,33]. The results show that at $100V$ such electric field transients begin to develop as the applied RF frequency is raised to higher values and its nature changes with the variation in the applied frequency. The frequencies of these transients are much higher than the applied RF frequency and are of the order of or higher than the electron plasma frequency (*i.e.* $f_{pe} = \sqrt{n_e e^2/\varepsilon_0 m_e}/2\pi$). These transients modify the bulk plasma properties as can be seen by the changes in the *electron energy distribution function* (EEDF). Such changes in the EEDF have been noted in some of the earlier experimental studies[38–41]. Sugai et al.[38–41] have observed that depending on the gas pressure, at 13.56 MHz driving frequency, a bi-Maxwellian (Maxwellian for non-Ramsauer gases) or convex type EEDF can occur. On the other hand, the VHF plasma excitation typically shows a bi-Maxwellian EEDF irrespective of the nature of gas (Ramsauer or non-Ramsauer) or gas pressure and is attributed to the higher collisionless heating in CCPs excited by the VHF. The simulation results for 100 mTorr does not compare favourably with the experimental observations of Sugai et al.[38]. In particular it does not reproduce the experimentally observed changes in the EEDF[42]. In a recent work[1], we have carried out a set of self-consistent particle-in-cell/ Monte-Carle collision (PIC/MCC) simulations to study the influence of the driving frequency (27.12-70 MHz) on the EEDF and the interaction of electrons with oscillating sheath in low pressure (5 mTorr) capacitive discharges. We considered a fixed discharge voltage of 100 V and simulated an argon plasma. A transition in EEDF from a strongly bi-Maxwellian (at 27.12 MHz) to a convex nature of distribution (at 50 MHz which is an intermediate frequency) and then ultimately a weakly bi-Maxwellian distribution at higher frequencies (above 50 MHz) was observed. Such transition appears to be due to the production of electric field transients or energetic electrons in the vicinity of the sheath edge that can transfer energy to the electrons of bulk plasma and alter the nature of the EEDF. For frequencies larger than the critical frequency (*i.e.* 50 MHz), these highly energetic electrons are confined among the two sheaths thereby increasing the probability of ionization. As a consequence, the low energy electron population rises rapidly and prevents the tranformation of the EEDF into a weakly bi-Maxwellian one. It is also

seen that the time average plasma density remains nearly constant and the effective electron temperature increases by two-fold up to the transition frequency, however, above the transition frequency the electron density increases quickly and the effective electron temperature (T_{eff}) decreases[1]. In our present study we extend our previous work that only looked at the effect of the applied frequency on the CCP dynamics (keeping all other parameters constant) to systematically explore the influence of other parameters like the applied voltage and the extent of gap between the electrodes on the formation of the electric field transients as well as the changes in the the bulk plasma properties of the discharge. The aim is to provide a comprehensive account of the discharge dynamics over a multi-parameter operational space.

The paper is organized in the following manner. Section II provides a description of the simulation technique, which employs the Particle-in-Cell/Monte Carlo collision (PIC/MCC) based method[43,44]. Further, section III describes the physical interpretation and discussion of the simulation results. Finally, a summary of the results is provided in the concluding section IV.

II. SIMULATION SCHEME AND PARAMETERS

We have simulated the single frequency capacitive discharge (voltage driven) with the well-established and tested $1D3V$, self-consistent, electrostatic, particle-in-cell (PIC) code that has been used earlier in several of our past studies[1,33]. The simulation technique is established on Particle-in-Cell/Monte Carlo collision (PIC/MCC) methods[43,44]. The PIC simulation proposes full kinetic evidence about plasma processes like the interaction of electrons with the oscillating radio-frequency sheaths and also about the loss of kinetic energy due to electron absorption at the walls and their trajectories etc. The code was developed at Dublin City University by Prof. Miles M. Turner and it is exploited in numerous research papers[1,45–51]. For a comprehensive description of the simulation technique the reader is referred to[52,53]. All essential particle reactions like electron-neutral (inelastic, ionization, and elastic) and ion-neutral (inelastic, charge exchange, and elastic) collisions are considered here for all simulation cases. However metastable pooling, partial de-excitation, multi-step ionization, super elastic collisions and further de-excitation are not the part of simulation for simplification purpose. In the simulations, the creation of two metastable states (*i.e.*

Ar*, Ar**) has been considered however these are not tracked for output diagnostics. A proper choice of spatial grid size (*i.e.* lesser than Debye length) and time step size (to resolve the electron plasma frequency) have been used in simulation to take care of the accuracy and stability criteria of the PIC simulation. It is assumed here that the electrodes have infinite dimensions and are planar and parallel to each other and, for our current analysis, are operated in the voltage driven mode. The surface of electrodes are entirely absorbing for both the ions and electrons. The creation of secondary electron emission is also ignored here. The gap between the electrodes (the simulation space) is divided into 512 numbers of grids. We have taken 100 particles per cell for all sets of simulation. The temperature of neutral gas is *i.e.* 300 K which is similar to that of ions and the background neutral gas is uniformly distributed. In our set up, one electrode is grounded and the powered electrode is driven by following waveform:

$$V_{rf}(t) = V_0 sin(2\pi f_{rf} t + \phi) \tag{1}$$

A schematic diagram of the CCP discharge is shown in Fig.1. The amplitude of the discharge voltage is varied from 50 V to 150 V and the neutral gas pressure is 5 mTorr for all cases. All the cases were run for several hundred RF cycles to achieve steady state.

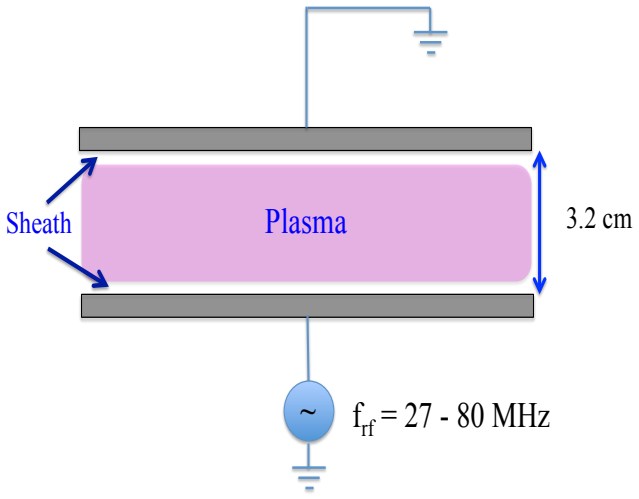

FIG. 1. Schematic diagram of symmetric single frequency CCP system.

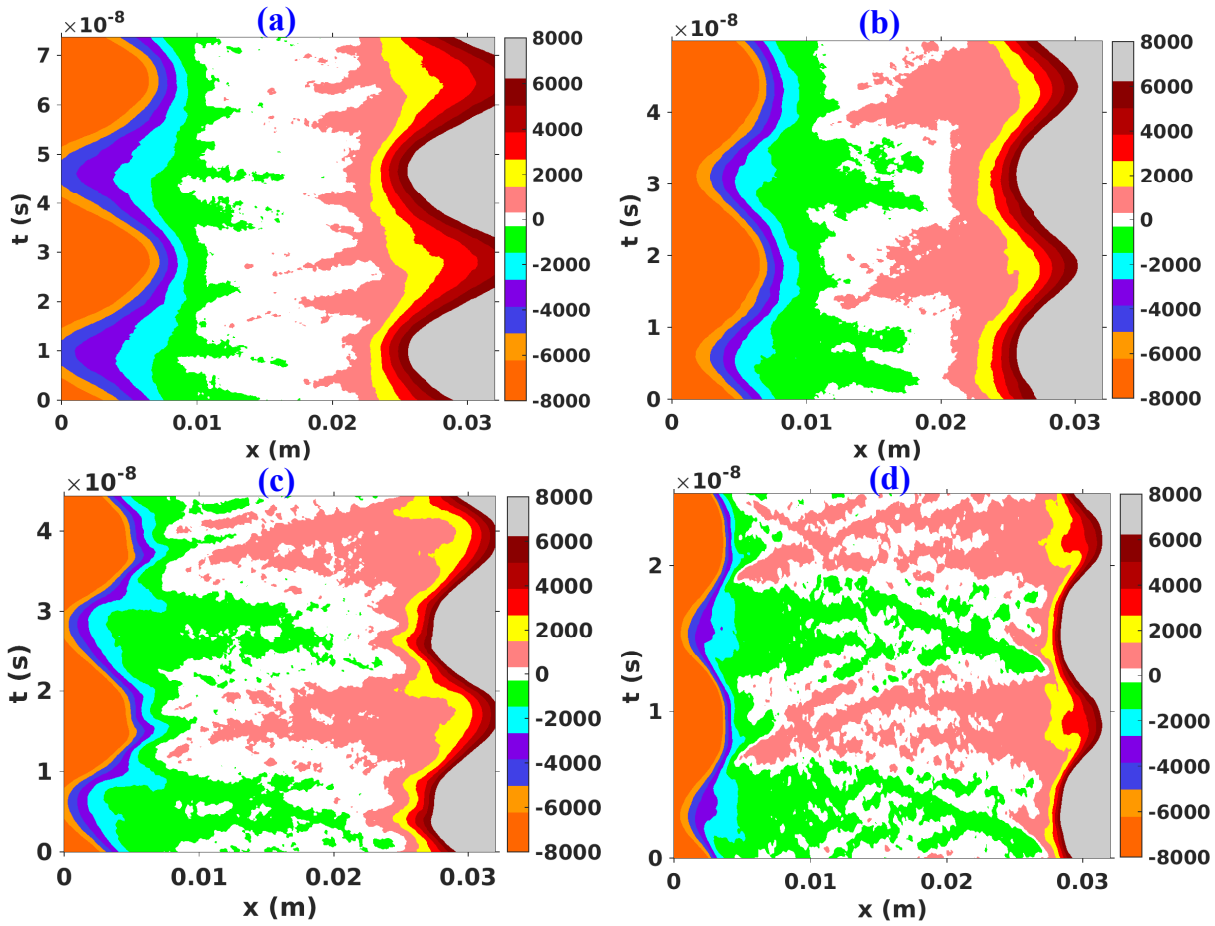

FIG. 2. Electric field evolution in space and time in the discharge gap at a) 27.12 MHz b) 40 MHz c) 45 MHz and d) 80 MHz driving frequency for fixed discharge voltage, 50 V.

III. SIMULATION RESULTS AND DISCUSSION

A. Driving frequency effect on electric field transients at different driving voltages

In this section we present the effect of driving frequency and discharge voltage on the electric field transients. The applied RF frequency is varied from 27.12 MHz to 80 MHz at three different driving voltages *i.e.* 50 V, 100 V and 150 V. As we discussed earlier, the formation of electric field transients at higher frequencies and at low pressure has been already reported recently[1,33]. The results demonstrate that at 100 V when the applied RF frequency varies from $27.12 - 80$ MHz, the transients do not exist at low frequency *i.e.* 27.12 MHz. However the transients appear at higher frequencies and its shape and size changes

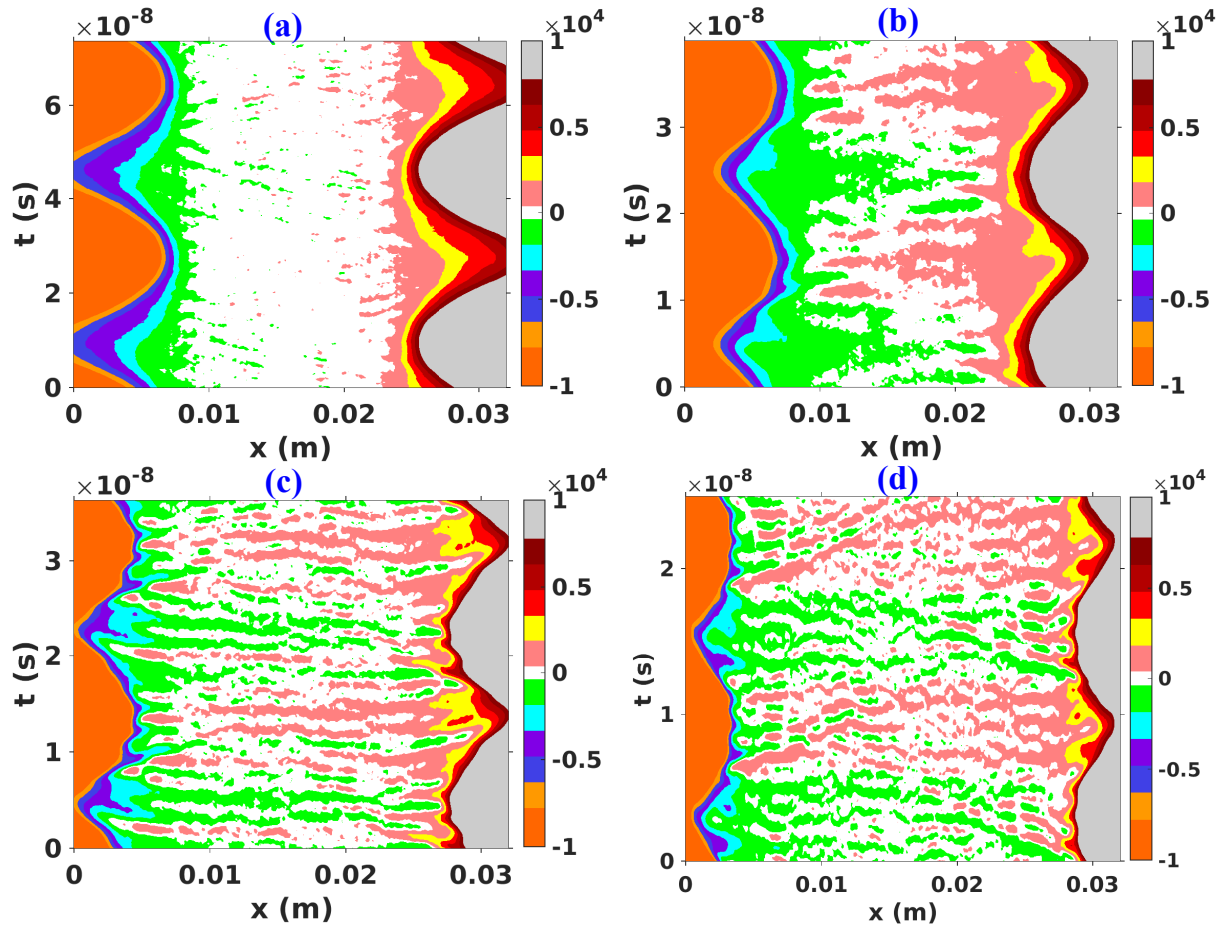

FIG. 3. Electric field evolution in space and time in the discharge gap at a) 27.12 MHz b) 50 MHz c) 55 MHz and d) 80 MHz driving frequency for constant discharge voltage, 100 V.

by changing driving frequency. We have observed in our present simulation results that the variation in applied voltage also changes the characteristics of transients drastically. Figure 2, 3 and 4, shows the spatio-temporal profile of the electric field (for last 2 RF cycles in steady state) for 4 different driving frequencies at 50 V, 100 V and 150 V respectively. These figures show that as we increase the driving frequency the electric field from the sheath region begins to penetrate inside the bulk plasma. Figure 2(a), 3(a) and 4(a) shows that at 27.12 MHz the electric field are mostly confined near to the sheath area. However, at transition frequency, *i.e.* 40 MHz (figure 2(b), 50 V), 50 MHz (figure 3(b), 100 V) and 55 MHz (figure 4(b), 150 V), there is a significant presence of electric field transients in the bulk plasma, though these field transients starting from one sheath do not hit the opposite sheath. The electric field in the bulk appears due to the transients excited by bursts of high-energy

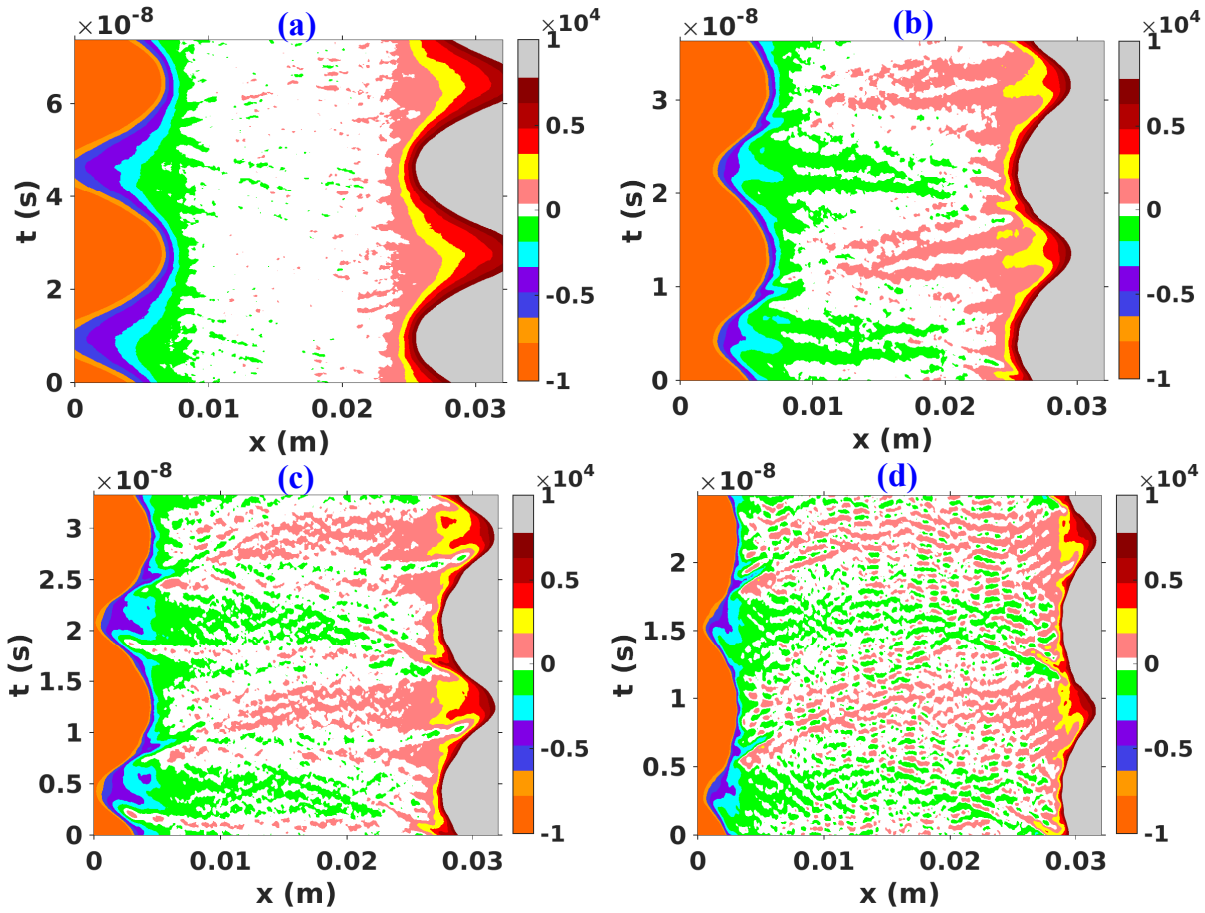

FIG. 4. Electric field evolution in space and time in the discharge gap at a) 27.12 MHz b) 55 MHz c) 60 MHz and d) 80 MHz driving frequency for fixed discharge voltage, 150 V.

electrons emitted from the sheath edge[30,54,55]. For low applied voltages ($|e\varphi(x)|/T_e \ll 1$) these transients act as linear excitations and phase mix in a distance of order v_{th}/ω_{rf}[1,16–18] where v_{th} is electron thermal velocity defined as $v_{th} = \sqrt{(2T_e/m_e)}$. However, when applied voltages are high enough ($|e\varphi(x)|/T_e \gg 1$) nonlinear processes affecting the electron energy distribution function (EEDF) become critical. We will discuss this in a later section. Above the transition frequency, figure 2(c, d), 3(c, d) and 4(c, d), it is observed that a substantial amplitude of high-frequency oscillations of the electric field occur at the interface of the sheath and boundary of bulk plasma.

Such a phenomenon can only arise from the presence of an electron flow coming from the bulk plasma to the sheath region and modifying the position of the sheath edge. The electrons are further reflected from the sheath on the fast electron quiver time and pushed back into the bulk plasma region. The expelled electrons gain or lose energy depending

on the phase of the oscillating sheath. The sheath expansion phases are shown in fig 2(c) right-side 16-24 ns and left-side 5-14 ns, fig 3(c) right-side 10-18 ns, left-side 3-10 ns which lead to net electron heating. In addition to transients in the sheath region one also finds simultaneous occurrence of local transient electric fields in the bulk region. The plasma is polarized because of these fields causing a bunching of the high-energy electrons in space and time. This in turn further boosts the modulation of the sheath edge. Such a self-sustaining mechanism underlies the process of the evolution of a perturbation to the high energy electrons[56].

One more important point to be noted is that as the applied voltage increases from 50 V to 150 V, the transient electric field structures, at and above transition frequency in each case, change in shape and nature. At 50 V the transient electric field structures are thick in shape, however, at 100 V the structures are relatively thin in shape and finally at 150 V it is observed that the field structures are like very fine threads or filaments. The number of filaments of electric field transient also increases as the applied frequency is further raised above the transition frequency.

Fig 5 shows the time evolution of electric field at the center of discharge and its Fast Fourier transform (FFT) for 50 V, 100 V and 150 V respectively. Two driving frequencies are shown at each driving voltage. The first driving frequency is the transition frequency and the second driving frequency is 80 MHz, which is well above the transition frequency. These FFT plots show the frequencies of the excited transients. Fig 5 (i, b) shows that at 50 V and 40 MHz the contribution of fundamental frequency is 30% and rest is in excitation of higher harmonics such as the 3^{rd} (*i.e.* 120 MHz) (dominant harmonic) and 5^{th} (*i.e.* 200 MHz). When the applied frequency is increased to 80 MHz at 50 V the excited transient frequencies shift towards the higher side and the fundamental frequency contribution decreases to 17% and higher harmonics like 3^{rd}, 5^{th}, 6^{th}, 7^{th} and 9^{th} harmonics are also excited. These harmonics have almost equal contribution and most dominant after the fundamental (see 5 (ii, b)). Similarly in fig 5 (iii, b), at 100 V and 50 MHz the dominant frequency is the fundamental frequency (*i.e.* 25%) with many higher harmonics like 2^{nd}, 3^{rd}, 5^{th} and 6^{th}. The 5^{th} harmonic (*i.e.* 250 MHz) is most dominant one after fundamental frequency. At 100 V, when applied frequency increased to 80 MHz (see 5 (iv)) the frequency of excited harmonics are much higher. Fig 5 (iv, b) shows that the contribution of fundamental frequency decreases to nearly half (*i.e.* 13%) and many higher harmonics

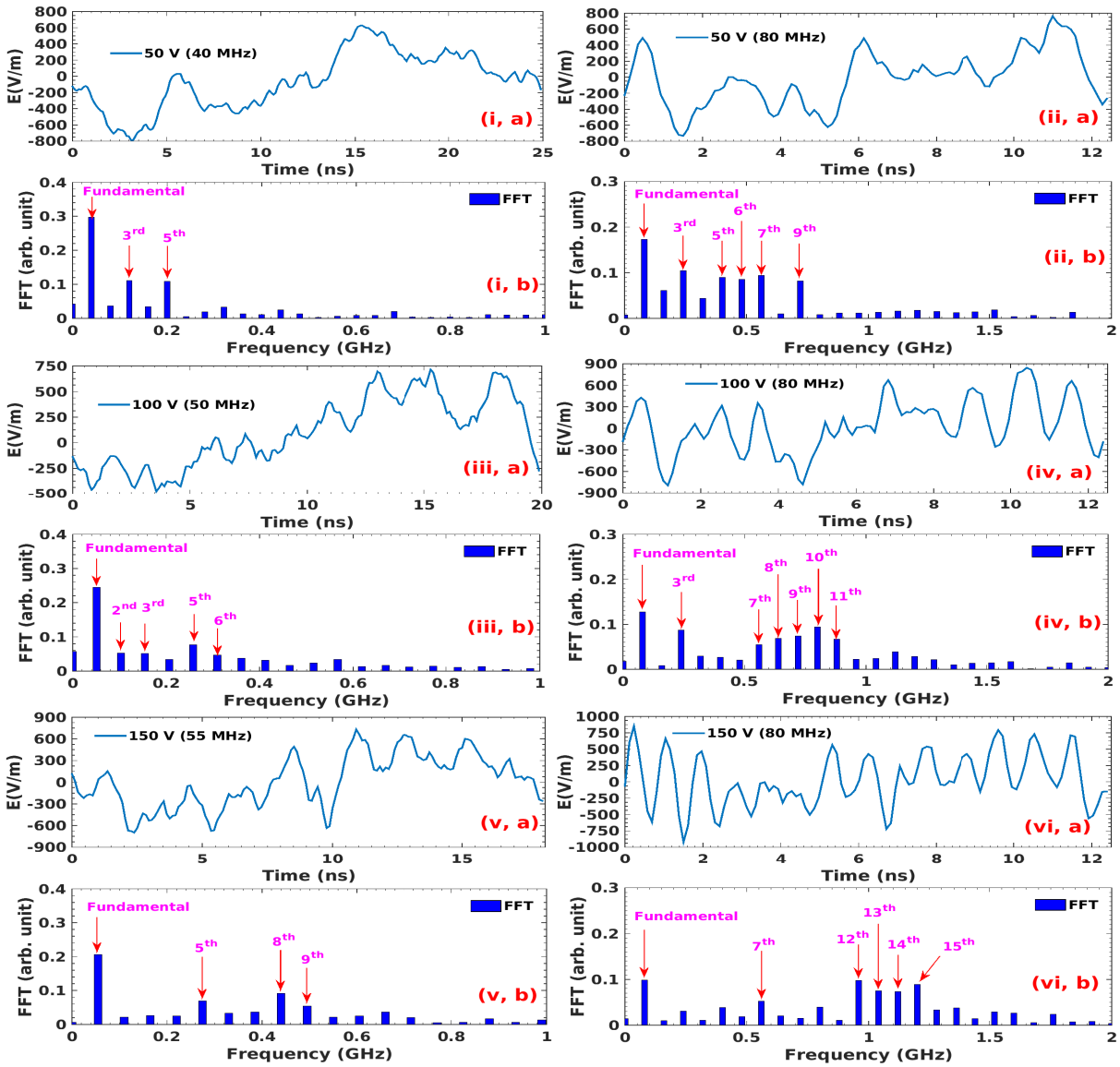

FIG. 5. Temporal evolution of electric field at the center of discharge and its Fast Fourier transform (FFT) for (i) 50 V (40 MHz) (ii) 50 V (80 MHz) (iii) 100 V (50 MHz) (iv) 100 V (80 MHz) (v) 150 V (55 MHz) (vi) 150 V (80 MHz).

like 3^{rd}, 7^{th}, 8^{th}, 9^{th}, 10^{th} and 11^{th} are present. The 10^{th} harmonics (*i.e.* 800 MHz) is the most dominant one with contribution of $\sim$ 10%. However the significant presence of other harmonics are also here. Again In fig 5 (v, b) *i.e.* 150 V and 55 MHz the fundamental frequency is most dominant with contribution of $\sim$ 21%. Other dominant excited harmonics after the fundamental are 5^{th} (*i.e.* 275 MHz), 8^{th} (*i.e.* 440 MHz) and 9^{th} (*i.e.* 495 MHz). When the applied frequency increases to 80 MHz (see fig 5 (vi, b)) the fundamental frequency

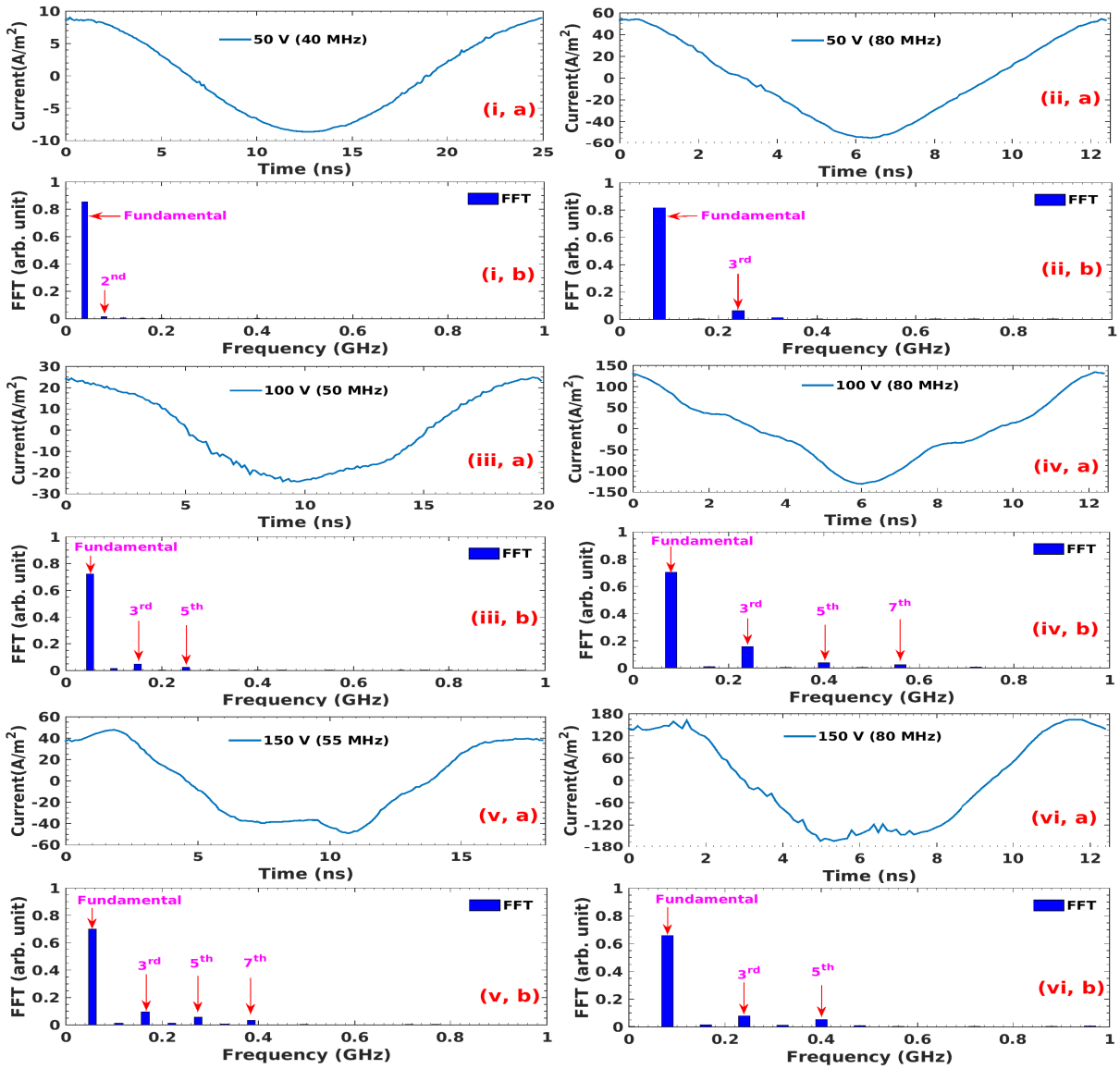

FIG. 6. Figure shows time evolution of electric current at the powered electrode and its Fast Fourier transform (FFT) for (i) 50V (40 MHz) (ii) 50V (70 MHz) (iii) 100V (50 MHz) (iv) 100V (70 MHz) (v) 150V (55 MHz) (vi) 150V (80 MHz).

contribution decreases significantly (*i.e.* 10%) with excitation of many higher harmonics like 7^{th}, 12^{th}, 13^{th}, 14^{th} and 15^{th}. We can see that 12^{th} (960 MHz), 13^{th} (1040 MHz), 14^{th} (1120 MHz) and 15^{th} (1200 MHz) are the most dominant one. From the above discussion we can make two conclusions: (a) the power in the excited harmonics get shifted towards a higher frequency side by increasing the voltage from 50 V to 150 V, (b) at all voltages, below the critical frequency (*i.e.* 40 MHz (50 V), 50 MHz (100 V) and 55 MHz (150 V))[33]

the fundamental frequency contribution is dominant and above the critical frequency the fundamental frequency contribution reduces significantly. It is also clear that the frequency of a few of the harmonics in each case is greater than the electron plasma frequency (at center of discharge) and is able to penetrate the bulk plasma. For example at 50 V and 40 MHz, f_{pe} at center of discharge is 155 MHz and the 5^{th} harmonic (200 MHz) is higher than f_{pe} and can penetrate the bulk. Similarly at 80 MHz and 50 V, f_{pe} at the center of discharge is 477 MHz and the dominant 6^{th} (480 MHz), 7^{th} (560 MHz) and 9^{th} (720 MHz) harmonics are higher than f_{pe}. It is true for other cases as well. The presence of higher harmonics in the electric field could lead to the generation of non-sinusoidal current waveform appearing at the powered electrode. Figure 6 demonstrates the current density from PIC simulation and their FFT at the powered electrode for the consistent 6 cases as shown in fig 5. We observe that the fundamental frequency contribution at 50 V and 40 MHz is 87% (refer fig 6 (i, b)) with negligible higher harmonics component. However when frequency is increased to 80 MHz (see fig 6 (ii, b)) the contribution of the fundamental frequency decreases to 81% and the presence of the 3^{rd} harmonic is visible. When the applied voltage increases to 100 V then at 50 MHz the fundamental frequency contribution is 74% (refer fig 6 (iii, b)) which is further decreased to 69% and the higher harmonic presence is significant (see fig 6 (iv, b)). Similarly at 150 V and 55 MHz the contribution of fundamental frequency is nearly 72% (see fig 6 (v, b)) and rest is in higher harmonics. When frequency is increased to 80 MHz the fundamental frequency contribution decreases to 63% and the remaining is in higher harmonics (see fig 6 (vi, b)). A similar type of higher harmonics in current profile were also reported by Wilczek et al.[37] for an asymmetric CCP voltage driven case. Thus, the presence of higher harmonics in the electric field inside the bulk plasma through non-linear sheath interaction also causes generation of the non-sinusoidal current waveform at the electrode with a significant amount of higher harmonic contents.

The above results demonstrate that the frequency of these transients changes significantly with an increase in the discharge voltage and consequently the properties of the bulk plasma are also modified drastically. The most efficient way to study the properties of plasma is the measurement of the EEDF.

Figure 7, 8 and 9, show the EEDF at the center of the discharge for fixed driving voltages of 50, 100 and 150 $Volt$ respectively. The two ranges of frequencies plotted in each figure (a) and (b), are based on the change in the heating mode transition as described in our

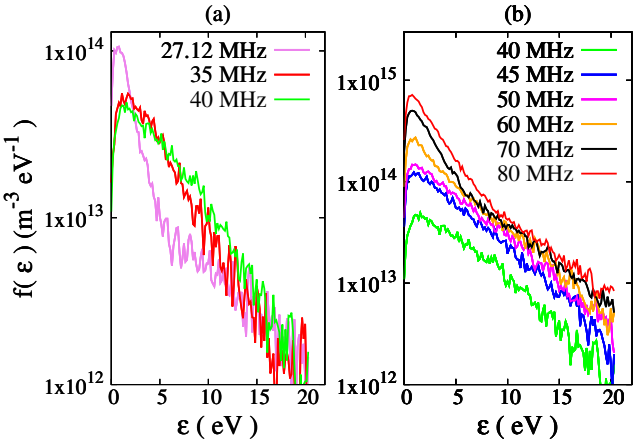

FIG. 7. For a constant discharge voltage 50 V, the EEDF at the center of the plasma discharge is shown for different driving frequencies a) 27.12 - 40 MHz b) 40 - 80 MHz.

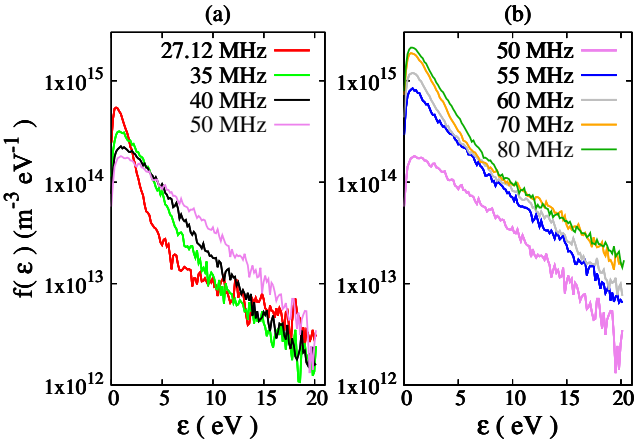

FIG. 8. For a constant discharge voltage 100 V, the EEDF at the center of the plasma discharge is shown for distinct driving frequencies a) 27.12 - 50 MHz b) 50 80 MHz.

previous paper[1]. The transition frequencies are 40 MHz, 50 MHz and 55 MHz respectively for the above defined voltages. As displayed in figure 7 (a), 8 (a) and 9 (a), below the transition frequencies, e.g. at 27.12 MHz, the EEDF is strongly bi-Maxwellian which has a large population of low energy electrons and the remaining electrons are in the high-energy tail. The low energy and high energy electron population is defined by the intersection of two slopes in the bi-Maxwellian distribution. The population of electrons below the intersection is considered as low energy electrons and the population of electrons above intersection is the high-energy tail. The intersection between the two slopes is observed at ~ 6 eV for all 3

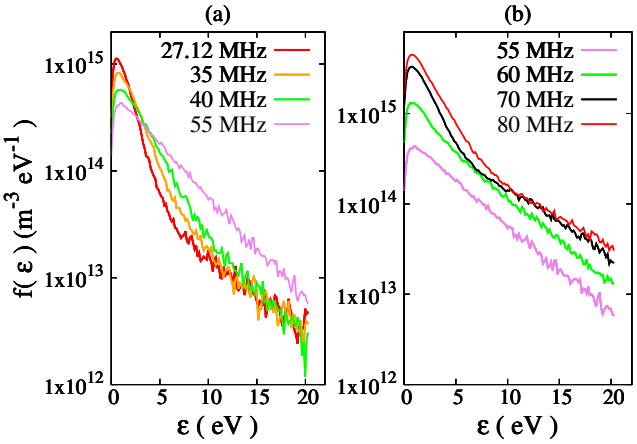

FIG. 9. For a fix discharge voltage 150 V, the EEDF at the center of the plasma discharge is shown for distinct driving frequencies a) 27.12 - 55 MHz b) 55 80 MHz.

different voltages. As shown in figure 7, 8 and 9, the population of low energy electrons at 27.12 MHz are $\sim 85\%$, $\sim 90\%$ and $\sim 94\%$ at 50, 100 and 150 V respectively. By increasing the driving frequency from 27.12 MHz to the transition frequency, the population of low energy electrons drop and the population of intermediate energy electrons, below ionization, increases. As a result, the structure of EEDF modifies from two-temperature form to a convex type structure. At the transition frequency the EEDF from simulation is fitted as per the following equation,

$$f(r) = A\left(\frac{E^r}{B}\right) \tag{2}$$

where A and B are constants and E is the electron energy. The curves from simulation at transition frequency for respective voltages are best fitted to a power function with exponents, $r \sim 1.59$ (50 V, 40 MHz),$r \sim 1.4$ (100 V, 50 MHz) and $r \sim 1.05$ (150 V, 55 MHz), and are therefore described as a convex type EEDF or nearly Maxwellain at 150 V and 55 MHz driving frequency.

As shown in figure 7 (b), 8 (b) and 9 (b), *i.e.* above the transition frequency, the population of both low-energy and high-energy electrons increases, however, the population of low-energy electrons increases at a much quicker rate when compared to high energy tail electrons and consequently the EEDF becomes again bi-Maxwellian. At 50, 100 and 150 V, the increase in low-energy electron population is $\sim 82\%$, $\sim 85\%$ and $\sim 88\%$, respectively at 80 MHz; however, the population of high-energy electrons increases by $\sim 18\%$, $\sim 15\%$

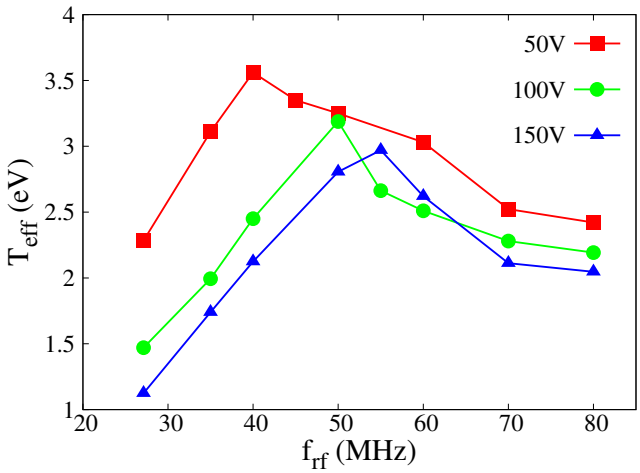

FIG. 10. Effective electron temperature (T_{eff}) versus driving frequency (f_{rf}) at the centre of the discharge for constant discharge voltages, $50 - 150$ V.

and $\sim 12\%$ respectively. Note that the increase in low and high-energy electron population is dependent on the discharge voltage. The percentage increase in the low-energy electron population increases with rise in discharge voltage, whereas, the percentage increase in the high-energy electron population decreases with an increase in discharge voltage.

At the driving frequency of 27.12 MHz the EEDF has a bi-Maxwellian character. Due to this the low energy electrons of Ramsauer gases (Ar) have a collisionless nature and oscillate without gaining any energy from the oscillating RF sheath. The tail high-energy electrons however can overcome the presence of ambipolar fields and get intensely heated by interacting with the oscillating nonlinear sheath electric field[57]. Figure 10 displays the effective electron temperature (T_{eff}) at the center of the discharge defined as below

$$f(r) = \left(\frac{2}{3}\right) \frac{\int \varepsilon F(\varepsilon) d\varepsilon}{\int F(\varepsilon) d\varepsilon} \tag{3}$$

where $F(\varepsilon)$ is the selfconsistent EEDF and ε is the electron energy obtained from the simulation. Figure 10 shows that the T_{eff} increases up to the transition frequency by less than two-fold (*i.e.* from 2.28 eV (at 27.12 MHz) to 3.56 eV (at 40 MHz)), two-fold (*i.e.* from 1.6 eV (at 27.12 MHz) to 3.2 eV (at 50 MHz)) and more than two-fold (*i.e.* from 1.22 eV (at 27.12 MHz) to 2.96 eV (at 55 MHz)) for 50 V, 100 V and 150 V respectively. Above the transition frequency, the T_{eff} drops back to 2.42 eV (50 V), 2.19 eV (100 V) and 2.04 eV (150 V), which is still higher compared to 27.12 MHz plasma excitation in each case (see figure 10).

This transformation leads to separation of the power deposited into various inelastic and ionizing collisions. In the case of 50 V, we have noticed a change in the inelastic collision rate (*i.e.* formation of metastable) from 5.2×10^{19} $m^{-3}s^{-1}$ (at 27.12 MHz) to 9.2×10^{19} $m^{-3}s^{-1}$ (at 40 MHz), although, the ionizing collisional rate changes relatively very little from $\sim 5.8 \times 10^{19}$ $m^{-3}s^{-1}$ (at 27.12 MHz) to $\sim 6.5 \times 10^{19}$ $m^{-3}s^{-1}$ (at 40 MHz) during this transition. It is observed that there is $\sim 77\%$ growth in inelastic collision rate (production of Ar^{*} and Ar^{**}) however the change in ionizing collisional rate is only $\sim 13\%$. Above the transition frequency both inelastic and ionizing collision rates rise rapidly. At 100 V the inelastic collision rate increases from 1.26×10^{20} $m^{-3}s^{-1}$ (at 27.12 MHz) to 2.2×10^{20} $m^{-3}s^{-1}$ (at 50 MHz), while, the ionizing collisional rate changes relatively less from $\sim 1.5 \times 10^{20}$ $m^{-3}s^{-1}$ (at 27.12 MHz) to $\sim 1.9 \times 10^{20}$ $m^{-3}s^{-1}$ (at 50 MHz) through this transition[33]. So there is $\sim 75\%$ growth in inelastic collision rate, however, the change in ionizing collisional rate is $\sim 27\%$. After the transition frequency both inelastic and ionizing collision rates grow rapidly. Finally at 150 V the inelastic collision rate rises from 1.75×10^{20} $m^{-3}s^{-1}$ (at 27.12 MHz) to 4.0×10^{20} $m^{-3}s^{-1}$ (at 55 MHz), though, the change in ionizing collisional rate is relatively less *i.e.* $\sim 2.1 \times 10^{20}$ $m^{-3}s^{-1}$ (at 27.12 MHz) to $\sim 2.95 \times 10^{20}$ $m^{-3}s^{-1}$ (at 55 MHz) across this transition. It is observed that there is $\sim 129\%$ growth in inelastic collision rate but the change in ionizing collisional rate is $\sim 40\%$. Above the transition frequency both inelastic and ionizing collision rates grow rapidly. The above observations show that at 50 V and 100 V the inelastic collision rates are of the same order while the ionizing collisional rates nearly double. However, at 150 V, the inelastic collision rate increases much faster compared to the ionizing collisional rate in contrast to the situation at 100 V. So the production of metastables would be much higher at higher voltages. Figure 11 represents the time-averaged heating $< J.E >$ at different applied frequencies for 50 V, 100 V and 150 V. It is important to note that below the transition frequency (*i.e.* 40 MHz (50 V), 50 MHz (100 V) and 55 MHz (150 V)) electron heating appears predominantly in the vicinity of the sheath edge, and the electron cooling *i.e.* negative $< J.E >$ (maximum -630 W/m^3 at 40 MHz (50 V), -1130 W/m^3 at 50 MHz (100 V), -1800 W/m^3 at 55 MHz (150 V)), in the bulk plasma (inset of figure 11 (a), (b) and (c)) which increases with frequency[17,21]. The electron cooling effect inside the bulk plasma results from an electric field in the bulk operating in opposition to the fast electrons created from sheath, as well as phase-mixing between bulk plasma electrons and tail electrons. Above the transition frequency, the region

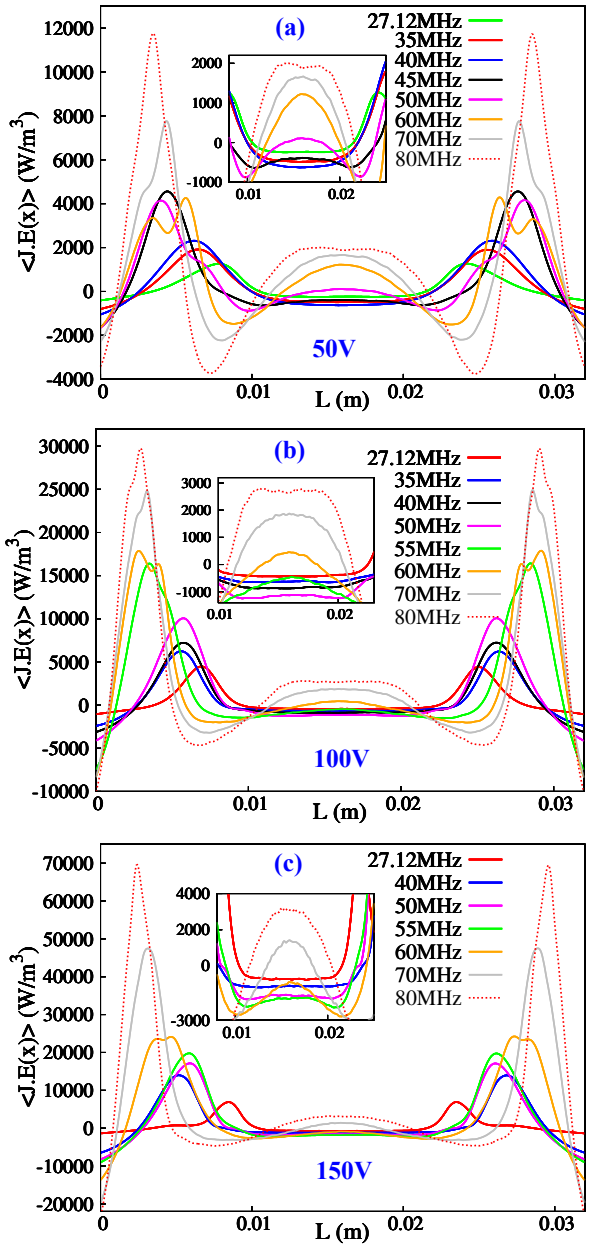

FIG. 11. Time average electron heating ($< J.E >$) in the discharge for different driving frequencies and for constant discharge voltages of (a) 50 V, (b) 100 V and (c) 150 V.

of sheath heating moves nearer to the plasmas boundary as the sheath-width reduces due to increase in plasma density and the electron heating near the sheath edge continues to increase with the driving frequency. Additionally, positive $< J.E >$ (inset of Fig. 11) is observed in the bulk plasma (maximum 2000 W/m^3 (at 80 MHz, 50 V), 2700 W/m^3 (at 80 MHz, 100 V) and 3135 W/m^3 (at 80 MHz, 150 V)). Physically this phenomenon may be

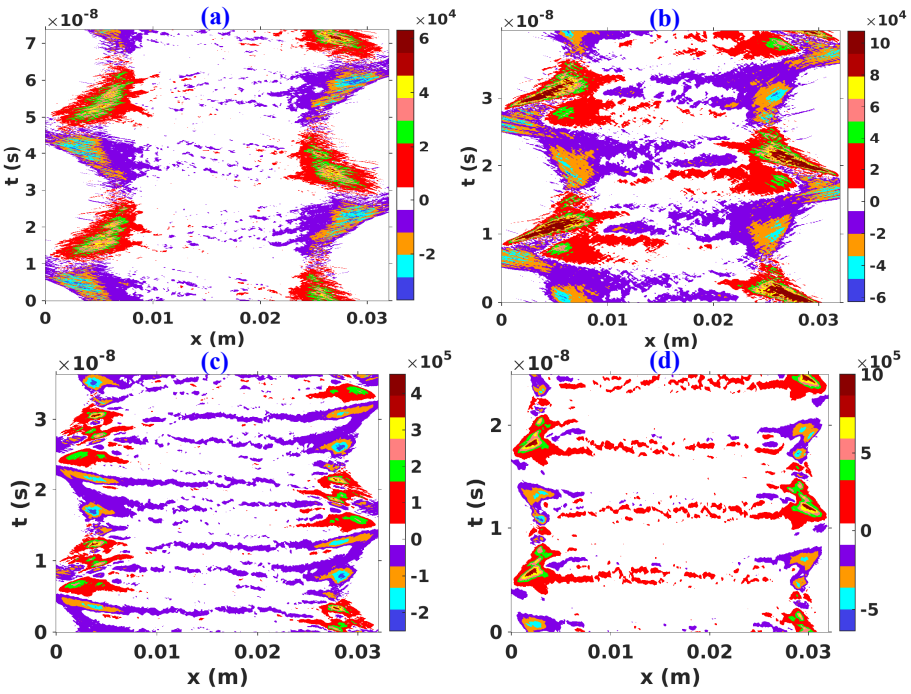

FIG. 12. Above figure shows the spatio-temporal profile of electron plasma heating ($J.E$) in the discharge for 4 different driving frequencies (a) 27.12 MHz (b) 50 MHz (c) 55 MHz (d) 80 MHz and for a fixed driving voltage of 100 V.

elucidated as follows: the disturbances at the plasma-sheath boundary inject transients or pulses of energetic/hot electrons into the bulk plasma. In the absence of electric fields, these transients penetrate into the bulk plasma and generate electron current density there.

Conservation of the total current dictates the amount of current produced by the electric field. Electric field self-consistently modifies itself to fulfil this constraint. Thus the electric field could be of either sign and lead to positive or negative bulk heating. The phase of the transient electric fields with respect to the total current varies with the applied frequency. So this can lead to changes in the sign of the bulk plasma heating as a function of applied frequency. Thus near a positive $< J.E >$ region there can be an area of strong electron cooling from the reflected, bunched electrons interacting with the bulk plasma. Such a mechanism could be responsible for the instantaneous sheath edge oscillations and the plasma polarization electric field within bulk plasma. To visualize the electron heating and cooling effect we have plotted the spatio-temporal profile of $J.E$ for 100 V in fig 12 at 4 different applied frequencies for last two RF cycles. Here in figure 12 (a) and (b) indicates that the heating mostly occurs near the sheath edge and negative heating or electron cooling

appears inside the bulk. The magnitude of negative heating is also more in (b) compared to (a). However in figure 12 (c) the heating is still negative inside bulk but now its magnitude is less compared to (b) and lastly in (d) there is an appearance of positive electron heating inside bulk. Not shown here but similar trend is also observed at 50 V and 150 V.

B. Effect of electrode gap on electric field transients

System length or the gap between electrodes is one of the crucial parameters which affects the transient characteristics significantly. As we have seen in our previous discussion that at 100 V the transients hit the opposite sheath at 55 MHz for an electrode gap of 3.2 cm . To study the effect of system length on electric field transients we have carried out simulations with three different system lengths, namely, 2.5 cm, 3.2 cm and 4 cm at 100 V discharge voltage and 55 MHz driving frequency. The electric field transients for these 3 cases are shown in figure 13.

Fig 13 (a) shows that for a 2.5 cm electrode gap the electric field transients start from the sheath and penetrate the bulk plasma but do not reach the opposite sheath. The transients are thick and the sheath edges are smooth. When the electrode gap is increased to 3.2 cm (see Fig 13 (b)) the transients are thinner and more in number compared to the 2.5 cm case. These transients hit the opposite sheath and modify the instantaneous sheath edge, which is clearly visible in Fig 13 (b). When the electrode gap is further increased to 4 cm , the transients are thin, discontinuous and are not able to hit the opposite sheath so the sheath edges are almost smooth (see Fig 13 (c)). It is clear that the nature of these transients is a function of the electrode gap.

Fig 14 (i)-(iii) shows the time evolution of the electric field at the center of the discharge and its FFT for electrode gaps of 2.5 cm, 3.2 cm and 4 cm respectively. In figure 14 (i, b) the FFT of electric field at 2.5 cm shows that the contribution of fundamental frequency is 22%. The other dominant higher harmonics are 3^{rd}, 5^{th} and 6^{th} with a small presence of higher harmonics. Here the electron plasma frequency *i.e.* f_{pe} at the center of discharge is $\sim$ 356 MHz so higher harmonics like 6^{th} and above can only penetrate up to the center of discharge. Figure 14 (ii, b) demonstrates that when the electrode gap is increased to 3.2 cm the contribution of the fundamental frequency is decreased to $\sim$ 11%. The other most influential higher harmonics after the fundamental are the 3^{rd}, 5^{th}, 7^{th}, and 10^{th}.

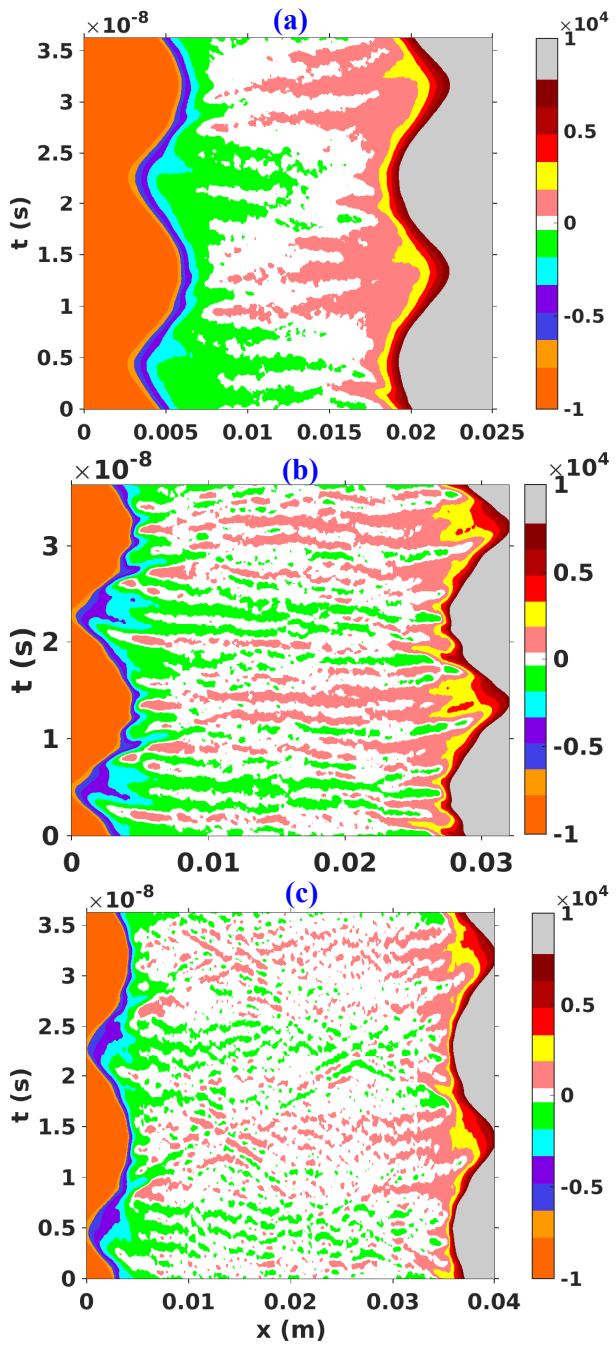

FIG. 13. Spatio-temporal profile of electric field for different electrode gap (a) 2.5 *cm* (b) 3.2 *cm* (c) 4.0 *cm* at 55 MHz driving frequency and 100 V discharge voltage.

The contribution of 10^{th} harmonic is maximum *i.e.* $\sim$ 15%. The f_{pe} at center of bulk is $\sim$ 448 MHz so the 10^{th} harmonic and higher can penetrate through the bulk and hit the opposite sheath. When the electrode gap is further increased to 4 *cm* (see 14 (iii, b)), the contribution of the fundamental frequency is nearly same *i.e.* 10%. The other dominating

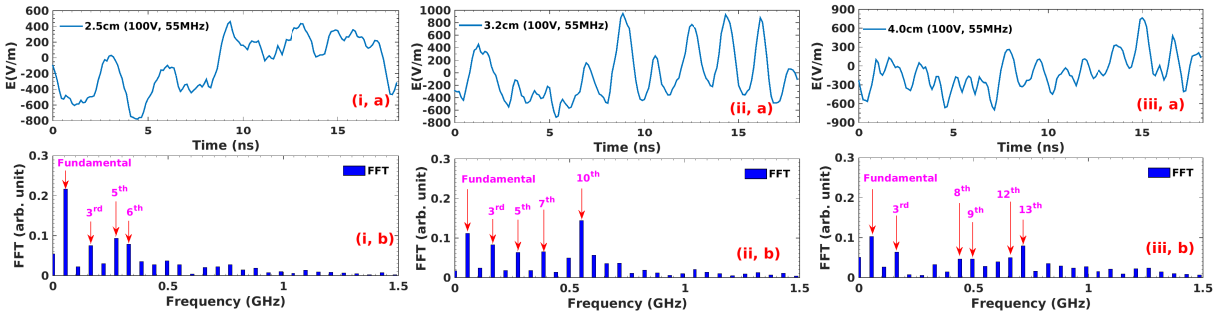

FIG. 14. Temporal evolution of electric field at the center of discharge and its Fast Fourier transform (FFT), for altered electrode gap (i) 2.5 *cm* (ii) 3.2 *cm* and (iii) 4.0 *cm* at 55 MHz driving frequency and 100 V discharge voltage.

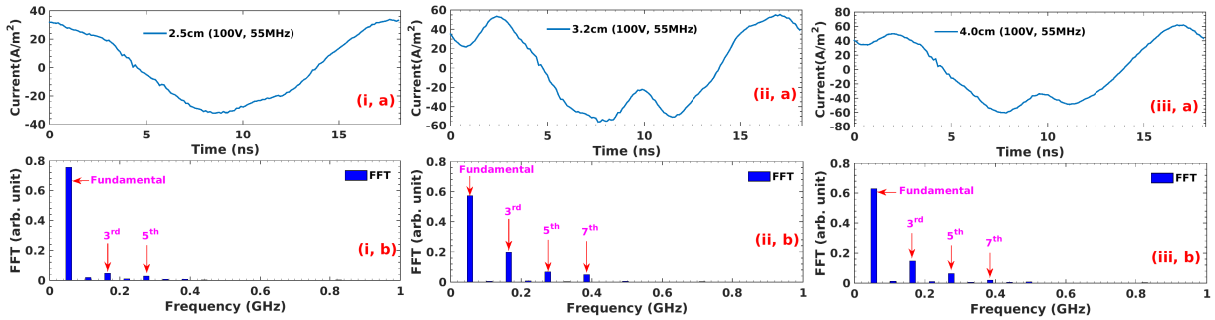

FIG. 15. Temporal evolution of electric current density at the powered electrode and its FFT for different electrode gap (i) 2.5 *cm* (ii) 3.2 *cm* and (iii) 4.0 *cm* at 55 MHz driving frequency and 100 V discharge voltage.

higher harmonics are 3^{rd}, 8^{th}, 9^{th}, 12^{th} and 13^{th}. The 13^{th} harmonic has more contribution after fundamental with 8% share. The f_{pe} at the center of discharge is $\sim$ 640 MHz here and the harmonics higher than 11^{th} harmonic can penetrate the bulk. As we have discussed earlier, generation of electric field transients is deeply associated with the non-sinusoidal current formation at powered electrode. Fig 15 (i)-(iii) shows the time evolution of the electric current density at the powered electrode and its corresponding FFT for the electrode gaps of 2.5 *cm*, 3.2 *cm* and 4 *cm* respectively. It is observed that the fundamental frequency contribution in 2.5 *cm* is $\sim$ 75% (refer 15 (i, b)) and the presence of higher harmonics are very weak. When the electrode gap is increased to 3.2 *cm* the fundamental frequency contribution decreases to $\sim$ 56% and the 3^{rd} (20%), 5^{th} (7%) and 7^{th} (5%) harmonics are clearly visible (see 15 (ii, b)). At the end when the electrode gap is further increased to

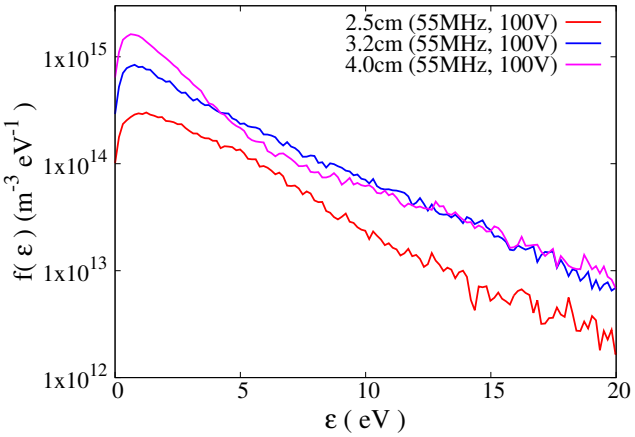

FIG. 16. EEDF at the center of the discharge for a fixed discharge voltage, 100 V, and driving frequency (55 MHz) for different electrode gap 2.5 *cm*, 3.2 *cm* and 4.0 *cm*.

4 *cm* the fundamental frequency contribution again increases to $\sim$ 63% and the higher harmonic contribution *i.e.* 3^{rd} (15%), 5^{th} (6%) and 7^{th} (2%) decreases (15 (iii, b)). The results conclude that the strength (amplitude) and number of higher harmonic contents (non-linearity) in the electric field is highest for an optimized discharge gap, which is 3.2 cm in this case. The corresponding amplitude of fundamental driving frequency in the current density at the electrode is also smallest and conversely the higher harmonic contents are maximum for this discharge gap.

The effect of the discharge gap and the generation of higher harmonics on the bulk plasma properties has been examined by studying the shape of the EEDF at the center of discharge. Figure 16 displays the EEDF at the center of discharge for all these 3 discharge gaps. It is clear that the EEDF is nearly Maxwellian for an electrode gap of 3.2 *cm*. When the gap increases to 4 *cm* the EEDF transforms to a bi-Maxwellian type while when the gap decreases to 2.5 *cm* again the shape of EEDF is non Maxwellian. It is important to note that when electrode gap increases from 2.5 *cm* to 3.2 *cm* the bulk plasma density with tail end electron population goes up. However when the electrode gap is further increased from 3.2 *cm* to 4.0 *cm*, the tail end electron population is almost same. Here the bulk density increases and the population of electron having energy between 4 eV to 10 eV slightly decreases. This transformation of EEDF is associated to the change in the nature of the electric field transients and thus the bulk properties of plasma are significantly affected by the nature of these transients.

IV. CONCLUSION AND DISCUSSION

In summary, we have carried out 1D-3V, self-consistent electrostatic particle-in-cell simulations to study the dynamics of voltage driven symmetric CCP Ar discharges over a range of discharge voltages, electrode gaps and driving frequencies to study the influence of these parameters on the electric field transients and bulk plasma properties. Our simulations show that all these three parameters have an influence on the nature of the transients and consequently on the bulk plasma properties. In the cases when the applied frequency is varied for individual cases at 3 different discharge voltages *i.e.* 50 V, 100 V and 150 V, it is observed that the nature of the electric field transients changes significantly particularly in their ability to move away from the sheath region and penetrate the bulk plasma. One also notices major changes in the shapes and sizes of these transients with higher frequencies transforming them to thinner and finer shapes. Such changes in the shapes of the transients are also brought by changes in the applied voltages at a fixed frequency with the higher voltages causing fine filament type structures. At a constant voltage, the FFT of electric field evolution at the center of discharge shows that when the rf frequency is varied from lower to higher values the contribution of the fundamental frequency decreases and higher harmonics play a significant role in the dynamics. At higher discharge voltage and higher driving frequency the higher harmonic contributions become dominant and trigger intense transients in electric field by nonlinear interaction with the oscillations of the rf sheath. We also find that the presence of higher harmonics in the electric field is deeply associated with the generation of non-sinusoidal current wave-forms generated at the powered electrode. Such changes are also seen as a function of the discharge gap. The changes in the frequencies of the transients also lead to important changes in the bulk properties of the plasma. We have observed these changes by looking at the changes in the EEDF in the various parametric regimes. We find that the shape of the EEDF changes from a bi-Maxwellian to a convex shape and finally to a bi-Maxwellian shape when the applied frequency is varied from 27.12 MHz to 80 MHz at 50 V, 100 V and 150 V. The effective electron temperature (T_{eff}) also changes drastically. It is found that the electron heating at the center of the discharge is positive at higher frequencies for all the voltages and a filamentation process is also observed in the spatio-temporal profile of the electron heating.

Our simulation results thus provide a comprehensive picture of the dynamical properties

of a collisionless CCP discharge as a function of three controllable external parameters, namely, the applied voltage, the applied frequency and the electrode gap distance. As we have shown, these parameters can significantly influence the shape, size and dynamical properties of the electric field transients that play an important role in determining the edge and bulk properties of the discharge. A judicious choice of the above three parameters can thus provide a means of controlling the nature of the plasma discharge and thereby its functional utility for various practical applications.

REFERENCES

[1]S. Sharma, N. Sirse, P. K. Kaw, M.M. Turner and A. R. Ellingboe, Physics of Plasmas 23, 110701 (2016).

[2]M. A. Lieberman, IEEE Trans. Plasma Sci. 16, 638 (1988).

[3]M. A. Lieberman and V. A. Godyak, IEEE Trans. Plasma Sci. 26, 955 (1998).

[4]V. A. Godyak, Sov. Phys.Tech. Phys. 16, 1073 (1972).

[5]O. A. Popov and V. A. Godyak, J. Appl. Phys. 57, 53 (1985).

[6]I. D. Kaganovich, Phys. Rev. Lett. 89, 265006 (2002).

[7]M. M. Turner, Phys. Rev. Lett. 75, 1312 (1995).

[8]E. Kawamura, M. A. Lieberman and A. J. Lichtenberg, Phys. Plasmas. 13, 053506 (2006).

[9]S. Sharma, Investigation of ion and electron kinetic phenomena in capacitively coupled radio-frequency plasma sheaths: A simulation study, Ph.D. thesis (Dublin City University, 2013).

[10]S. Sharma and M. M. Turner, J. Phys. D: Appl. Phys. 46, 285203 (2013).

[11]G. Gozadinos, M. M. Turner and D. Vender, Phys. Rev. Lett. 87, 135004 (2001).

[12]J. Schulze, B. G. Heil, D. Luggenholscher, T. Mussenbrock, R. P. Brinkmann, and U. Czarnetzki, J. Phys. D: Appl. Phys. 41, 042003 (2008).

[13]T. Mussenbrock and R. P. Brinkmann, Appl. Phys. Lett. 88, 151503 (2006).

[14]S. Sharma and M. M. Turner, Plasma Sources Sci. Technol. 22(3), 035014 (2013).

[15]J. Schulze, B. G. Heil, D. Luggenholscher, R. P. Brinkmann, and U. Czarnetzki, J. Phys. D: Appl. Phys. 41, 195212 (2008).

[16]S. Sharma, S. K. Mishra, and P. K. Kaw, Phys. Plasmas 21, 073511 (2014).

[17]I. D. Kaganovich, O. V. Polomarov and C. E. Theodosiou, IEEE Trans. Plasma Sci. 34,

696 (2006).

[18]S. Sharma, S. K. Mishra, P. K. Kaw, M. M. Turner and S. K. Karkari, Contrib. Plasma Phys. 55(4), 331 (2015).

[19]A. E. Wendt and W. N. G. Hitchon, J. Appl. Phys. 71, 4718 (1992).

[20]S. Sharma and M. M. Turner, Phys. Plasmas 20, 073507 (2013).

[21]M. Surendra and D. B. Graves, IEEE Trans. Plasma Sci. 19, 144 (1991).

[22]M. M. Turner, J. Phys. D: Appl. Phys. 42, 194008 (2009).

[23]T. Lafleur and P. Chabert, Plasma Sources Sci. Technol. 24(2), 044002 (2015).

[24]S. Sharma, S. K. Mishra, P. K. Kaw, A. Das, N. Sirse, and M. M. Turner, Plasma Sources Sci. Technol. 24(2), 025037 (2015).

[25]Ki Seok Kim, Nishant Sirse, Ki Hyun Kim, Albert Rogers Ellingboe, Kyong Nam Kim and Geun Young Yeom, J. Phys. D: Appl. Phys. 49, 395201 (2016).

[26]A. A. Howling, J. L. Dorier, C. Hollenstein, U. Kroll and F. Finger F, J. Vac. Sci. Technol. A 10, 1080 (1992).

[27]M. Surendra M and D. B. Graves, Appl. Phys. Lett. 59, 2091 (1991).

[28]E. Monaghan, T. Michna, C. Gaman, D. O'Farrel, K. Ryan, D. Adley, T. S. Perova, B. Drews, M. Jaskot and A. R. Ellingboe, Thin Solid Films 519, 6884 (2011).

[29]Ki Seok Kim, Ki Hyun Kim, You Jin Ji, Jin Woo Park, Jae Hee Shin, Albert Rogers Ellingboe and Geun Young Yeom, Scientific Reports 7, 13585 (2017).

[30]S. Wilczek, J. Trieschmann, J. Schulze, E. Schuengel, R. P. Brinkmann, A. Derzsi, I. Korolov, Z. Donko, and T. Mussenbrock, Plasma Sources Sci. Technol. 24, 024002 (2015).

[31]Rauf Shahid, Bera Kallol and Collins Ken, Plasma Sources Sci. Technol. 19, 015014 (2010).

[32]J. Schulze, A. Derzsi, K. Dittmann, T. Hemke, J. Meichsner, and Z. Donko, Phys. Rev. Lett. 107, 275001 (2011).

[33]Sarveshwar Sharma, Abhijit Sen, N. Sirse, M.M. Turner and A. R. Ellingboe, Physics of Plasmas 25, 080705 (2018).

[34]Sarveshwar Sharma, N. Sirse, A. Sen, J. S. Wu, and M.M. Turner, J. Phys. D: Appl. Phys. 52, 365201 (2019).

[35]P. A. Miller, E. V. Barnat, G. A. Hebner, P. A. Paterson and J. P. Holland, Plasma Sources Sci. Technol. 15, 889-99 (2006).

[36]R. R. Upadhyay, I. Sawada, P. L. G. Ventzek and L. L. Raja, J. Phys. D: Appl. Phys. 46, 472001 (2013).

[37]S. Wilczek, J. Trieschmann, J. Schulze, Z. Donko, R. P. Brinkmann, and T. Mussenbrock, Plasma Sources Sci. Technol. 27, 125010 (2018).

[38]E. Abdel-Fattah and H. Sugai, Jpn. J. Appl. Phys. 42, 6569 (2003).

[39]E. Abdel-Fattah and H. Sugai, Appl. Phys. Lett. 83, 1533 (2003).

[40]E. Abdel-Fattah, M. Bazavan and H. Sugai, Phys. Plasmas 19, 113503 (2012).

[41]E. Abdel-Fattah and H. Sugai, Phys. Plasmas 20, 023501 (2013).

[42]H. Takekida and K. Nanbu, Jpn. J. Appl. Phys. 43, 3590 (2004).

[43]C. K. Birdsall, Plasma physics via computer simulation (Adam Hilger, Bristol, 1991).

[44]R. W. Hockney and J. W. Eastwood, Computer simulation using particles (Adam Hilger, Bristol, 1988).

[45]M. M. Turner, Plasma Sources Sci. Technol. 22, 055001 (2013).

[46]J. Conway, S. Kechkar, N. OConnor, C. Gaman, M. M. Turner, and S. Daniels, Plasma Sources Sci. Technol. 22, 045004 (2013).

[47]P. C. Boyle, A. R. Ellingboe, and M. M. Turner, Plasma Sources Sci. Technol. 13, 493 (2004).

[48]L. Lauro-Taroni, M. M. Turner, and N. StJ. Braithwaite, J. Phys. D: Appl. Phys. 37, 2216 (2004).

[49]M. M. Turner, A. W. Hutchinson, R. A. Doyle, and M. B. Hopkins, Phys. Rev. Lett. 76, 2069 (1996).

[50]S. Sharma, S. K. Mishra, P. K. Kaw, and M. M. Turner, PHYSICS OF PLASMAS 24, 013509 (2017).

[51]S. Sharma, N. Sirse, M. M. Turner and A. R. Ellingboe, Phys. of Plasmas 25, 063501 (2018).

[52]J. P. Verboncoeur, Plasma Phys. Controlled Fusion 47, A231 (2005).

[53]M. M. Turner, A. Derzsi, Z. Donk, D. Eremin, and S. J. Kelly, Phys. Plasmas 20, 013507 (2013).

[54]T. Gans, J. Schulze, D. OConnell, U. Czarnetzki, R. Faulkner, A. R. Ellingboe, and M. M. Turner, Appl. Phys. Lett. 89, 261502 (2006).

[55]J. Schulze, T. Gans, D. OConnell, U. Czarnetzki, A. R. Ellingboe, and M. M. Turner, J. Phys. D: Appl. Phys. 40, 7008 (2007).

[56]M. Surendra M and D. B. Graves D B, Phys. Rev. Lett. 66, 1469 (1991).

[57]V. A. Godyak and R. B. Piejak, Phy. Rev. Lett. 65, 996 (1990).